https://doi.org/10.3311/PPci.21562

Periodica Polytechnica Civil Engineering, 67(2), pp. 637–645, 2023

Robust Topology Optimization of Continuum Structures under the Hybrid Uncertainties: A Comparative Study

Seyyed Ali Latifi Rostami[1], Muxi Li[1], Amin Kolahdooz[2], Hayoung Chung[3], Jian Zhang[1*]

[1] Faculty of Civil Engineering and Mechanics, Jiangsu University, Zhenjiang 212013, China
[2] Faculty of Technology, School of Engineering and Sustainable Development, De Montfort University, Leicester, LE1 9BH, UK
[3] Faculty of Department of Mechanical Engineering, Ulsan National Institute of Science and Technology, Ulsan, 44919, South Korea
[*] Corresponding author, e-mail: jianzhang@ujs.edu.cn

Received: 19 November 2022, Accepted: 28 February 2023, Published online: 09 March 2023

Abstract

Due to the inevitable involvement of multisource uncertainties related to the load, material property and geometry in practical engineering designs, robust topology optimization (RTO) has recently attracted increasing attention to account for these uncertain effects. However, the majority of the existing RTO works are concerned with single source uncertainty, and very few studies have considered the multisource (hybrid) uncertainties simultaneously. To this end, a comparative study on the hybrid uncertainties (HU), i.e., material-loading, geometric-loading, material-geometric, and material-geometric-loading uncertainties, for RTO of continuum structures is presented in this paper. A truncated Karhunen-Loeve expansion is adopted for uncertainty representation and a sparse grid collocation method for uncertainty propagation of the objective function and constraints. Effects of the various HU on the compliance and robust design are comprehensively investigated and compared with the RTO models under individual component uncertainty using two continuum benchmarks. An important observation from the results is that the hybrid uncertainty model is a conservative state, and the resulting RTO designs tend towards those with loading uncertainty only.

Keywords

robust topology optimization, hybrid uncertainties, continuum structure, sparse grid collocation, Karhunen-Loeve expansion

1 Introduction

Topology optimization (TO) is an iterative numerical process to achieve the best material layout under given boundary conditions by optimizing a prescribed objective function with specific design constraints. The majority of the most studies for structural TO are based on the deterministic assumption [1]. However, in real applications, uncertainty is inevitably observed due to insufficient knowledge, production error, changeable environment, and so on [2, 3]. In this regard, the deterministic assumption may result in a topologically sensitive and vulnerable design, whose performance is often subject to variations when considering various uncertain factors. Therefore, there is a strong need to consider the effect of uncertainty on the optimal topology in structural design.

To account for different uncertainties in topology optimization TO, two major paradigms, reliability-based topology optimization (RBTO) [4–6] and robust topology optimization (RTO) [7], are often used.

RBTO aims to achieve a design with a targeted probability of failure and ensure that the conditions leading to catastrophe are unlikely to happen [8, 9]. RTO tries to optimize the objective performance while simultaneously minimizing its sensitivity with respect to uncertain parameters [10]. This paper is concerned only with the RTO under various kinds of uncertainties.

RTO under uncertainty is usually investigated according to the types of uncertain variables, e.g., the load, material property and geometry, respectively. Most of research in this field only considered one source of uncertainty such as Elishakoff et al. [11], Dunning et al. [12], Cai et al. [13], Latifi Rostami et al. [14], Guest and Igusa [15], Lógó [16, 17], and Lógó et al. [18] did research on load uncertainty. For RTO under uncertainty in material property, we can referred the following works: Tootkaboni et al. [19], da Silva and Cardoso [20], Agrawal et al. [21]. Zhang and Kang [22], Latifi Rostami and Ghoddosian [23, 24], Latifi Rostami et al. [25] and investigated the RTO problems with geometric uncertainties.

Cite this article as: Latifi Rostami, S. A., Li, M., Kolahdooz, A., Chung, H., Zhang, J. "Robust Topology Optimization of Continuum Structures under the Hybrid Uncertainties: A Comparative Study", Periodica Polytechnica Civil Engineering, 67(2), pp. 637–645, 2023. https://doi.org/10.3311/PPci.21562

Since most practical structural designs usually involve multisource uncertainties related to the load, material property and geometry, the combination of different sources of uncertainties, called hybrid uncertainty, has been recently introduced into the RTO area. Latifi Rostami and Ghoddosian [26] investigated the RTO under hybrid material and geometric uncertainties for continuum structures using stochastic collocation methods. He et al. [27] presented an ESO-based method for optimizing the dynamic properties including dynamic-compliance and eigenvalue of continuum structures with HU in material, geometry and boundary condition. Meng et al. [28] formulated a perturbation-based RTO model for continuum structures with hybrid material and geometric uncertainties represented by probabilistic and fuzzy variables. Bai and Kang [29] and Cheng et al. [30] proposed the RTO approaches for continuum and engineering structures under hybrid bounded uncertainties in load and material property.

As stated in the introduction and from the comparison of the references stated in the article, it can be seen that most of the articles have satisfactorily investigated the presence of a type of uncertainty in the optimization problem. But in nature, it is possible that there are several types of uncertainty in the problem at the same time. Therefore, investigating the simultaneous presence of several types of uncertainty in the optimization problem (RTO) can be challenging and interesting. As a result, in this article, it has been tried to address this issue as the main innovation of this research.

The remainder of this paper is organized as follows. The stochastic optimization methodology for RTO is detailed in Section 2. A comprehensive study on the effect of various HU on compliance and robust design is shown in Section 3 with numerical examples. Finally, conclusions are drawn in Section 4.

2 RTO methodology

2.1 Deterministic TO

A mathematical formulation of the deterministic TO for compliance minimization problem is expressed as:

$$\begin{aligned} &\min : f(\rho) = \boldsymbol{l}^T \boldsymbol{u}, \\ &\text{subject to} : \boldsymbol{K}\boldsymbol{u} = \boldsymbol{f}, \\ &: \frac{\sum_{i \in \mathrm{N}_e} \bar{\tilde{\rho}}_i v_i}{V} \le V^*, \\ &: 0 \le \rho_i \le 1 \forall i \in N_e, \end{aligned} \tag{1}$$

where $\boldsymbol{K}$, $\boldsymbol{u}$ and $\boldsymbol{f}$ are the stiffness matrix, displacement and applied load vectors, respectively. N_e is the index set of all elements, $\bar{\tilde{\rho}}_i$ describes the physical density related to each element, v_i is the volume of element i, V is the total volume of the design domain, and V^* is the prescribed volume fraction. For a minimum compliance design, $\boldsymbol{l} = \boldsymbol{f}$.

In this research, the design domain is discretized by square elements and a density-based method is followed to optimize the topology, meaning that each element is assigned a density. An improved SIMP method is used to express the Young's modulus of the i^{th} element E_i as follows:

$$E_i = E_{\min} + \bar{\tilde{\rho}}_i^{\,p} \left(E_0 - E_{\min} \right), \tag{2}$$

where E_0 is the stiffness of the solid phase, $E_{\min}$ is a very small stiffness assigned to the void region in order to prevent the stiffness matrix from being singular, and ρ is the penalization parameter. Thus, the individual element contributions to the stiffness matrix K are calculated as $K_i = E_i K_0$, in which K_0 is the element stiffness matrix for unit stiffness.

To eliminate instabilities such as checkered patterns and mesh dependency, a mesh-independent density filtering [28] is applied by defining the physical element density as a weighted average of the densities in its neighborhood. Denoted as $\tilde{\rho}_i$, the filtered density for element i is calculated as

$$\tilde{\rho}_i = \frac{\sum_{j \in \mathrm{N}_{e,i}} w\left(\boldsymbol{x}_j\right) v_j \rho_j}{\sum_{j \in \mathrm{N}_{e,i}} w\left(\boldsymbol{x}_j\right) v_j}, \tag{3}$$

where $N_{e,i}$ is the neighborhood set of elements lying within the filter domain of radius R for element i. The weighting function $w(\boldsymbol{x})$ is defined as

$$w\left(\boldsymbol{x}_j\right) = R - \left|\boldsymbol{x}_j - \boldsymbol{x}_i\right|, \tag{4}$$

where $\boldsymbol{x}_i$ and $\boldsymbol{x}_j$ contain the central coordinates of the design cells i and j, respectively. The derivative of the filtered density $\tilde{\rho}_i$ with respect to the design variables is calculated as

$$\frac{\partial \tilde{\rho}_i}{\partial \rho_i} = \frac{w\left(\boldsymbol{x}_j\right) v_j}{\sum_{j \in \mathrm{N}_{e,i}} w\left(\boldsymbol{x}_j\right) v_j}. \tag{5}$$

Density filtering ensures that mesh-independent designs can be achieved. Nevertheless, if the filtered density is used, a pattern of gray areas will be difficult to interpret, and any practical realization of the resulting design requires a black-and-white discrete solution. This issue can be resolved by threshold imaging techniques such as

the single-step Heaviside Projection method [31]. All values above the assumed threshold η are projected to 1, and the values below it to 0. An expression for the physical density utilized here is given as

$$\bar{\tilde{\rho}}_i = \frac{\tanh(\beta\eta) + \tanh\left[\beta\left(\tilde{\rho}_i - \eta\right)\right]}{\tanh(\beta\eta) + \tanh\left[\beta\left(1-\eta\right)\right]}, \tag{6}$$

where the parameter η changes within the range [0,1] and β, a parameter that controls the smoothness of the image function, starts from one and gradually increases during the optimization process. The derivative of the physical density $\bar{\tilde{\rho}}_i$ to the filtered density $\tilde{\rho}_i$ is calculated as

$$\frac{\partial\bar{\tilde{\rho}}_i}{\partial\tilde{\rho}_i} = \frac{\beta\left\{\operatorname{sech}\left[\beta\left(\tilde{\rho}_i - \eta\right)\right]\right\}^2}{\tanh(\beta\eta) + \tanh\left[\beta\left(1-\eta\right)\right]}. \tag{7}$$

The 0/1 projection $\bar{\tilde{\rho}}_i$ is a function of the filtered density $\tilde{\rho}_i$ and the sensitivities of the objective function (1) (Eq. (1)) with respect to the original design variables are calculated using the chain rule as Eq. (8):

$$\frac{\partial f}{\partial \rho_j} = \sum\nolimits_{i\in \mathrm{N}_{e,j}} \frac{\partial f}{\partial\bar{\tilde{\rho}}_i}\frac{\partial\bar{\tilde{\rho}}_i}{\partial\tilde{\rho}_i}\frac{\partial\tilde{\rho}_i}{\partial\rho_j}. \tag{8}$$

To update the design variables, an optimality criteria method [20] is employed using the information obtained from the sensitivity analysis of the objective and constraint functions.

2.2 Stochastic optimization

When the robust design is considered in the TO, the structural response $\boldsymbol{u}$ becomes a stochastic field, and the objective function in Eq. (1) is a random variable. The compliance objective function of the RTO model is usually given as follows:

$$\begin{aligned} &\min_{\rho} : f\left(\rho\right) = \mathbb{E}\left[C\right] + \kappa\sqrt{\mathrm{Var}\left[C\right]}, \\ &\text{subject to} : \mathbb{E}\left[V\left(\rho\right)\right] \le V^*, \\ &\qquad\qquad : 0 \le \rho_i \le 1 \;\forall\; i \in \mathrm{N}_e, \end{aligned} \tag{9}$$

where $\mathbb{E}\left[C\right]$ is the mean value of the compliance, Var[C] is the compliance variance, and κ is a user-defined weighting coefficient. If there is no uncertainty in loading, the expected value and variance of the compliance can be obtained as:

$$\begin{aligned} &\mathbb{E}\left[C\right] = \mathbb{E}\left[\boldsymbol{f}^T\boldsymbol{u}\right] = \boldsymbol{f}_0^T\mathbb{E}\left[\boldsymbol{u}\right], \\ &\mathrm{Var}\left[C\right] = \mathrm{Var}[\boldsymbol{f}^T\boldsymbol{u}]. \end{aligned} \tag{10}$$

The sensitivities of the objective function in Eq. (9) with respect to the design variables $\boldsymbol{\rho}$ are found using the adjoint method [29]:

$$\frac{\partial f}{\partial\boldsymbol{\rho}} = \frac{\partial\mathbb{E}\left[C\right]}{\partial\boldsymbol{\rho}} + \kappa\frac{\partial\left(\sqrt{\mathrm{Var}\left[C\right]}\right)}{\partial\boldsymbol{\rho}}. \tag{11}$$

In the following subsections, the representation of the uncertainties as a stochastic field is first discussed. Then, the solution to the stochastic state problem using the probabilistic collocation method is presented in more detail.

2.2.1 Uncertainty representation

To model the random field (uncertain parameter) Z, a truncated Karhunen-Loeve expansion (KLE) is adopted, which can be defined by a square exponential correlation function $R_{yy'}$ as follows [32]:

$$R_{yy'} = \exp(-\frac{d^2}{2l_c^2}), \tag{12}$$

where $d = |y - y'|$ is the distance between the centers of two elements, and l_c is the correlation length. To generate the expansion analysis, the following Eq. (13) can be created using n eigenvalue-eigenvector pairs of the correlation matrix, i.e., (λ_i, γ_i):

$$Z\left(\rho,\zeta\right) = \sum\nolimits_{i=1}^{n}\sqrt{\lambda_i}\gamma_i\left(\rho\right)\varphi_i\left(\zeta\right) \approx \sum\nolimits_{i=1}^{n_{mode}}\sqrt{\lambda_i}\gamma_i\left(\rho\right)\varphi_i\left(\zeta\right), \tag{13}$$

where φ_i is a random variable. For dimension reduction, the expansion is truncated up to the first $n_{mode} < n$ modes. Stochastic variables are assumed to have a uniform distribution with zero mean and unit variance, i.e., $\varphi_i\left(\zeta\right) = \zeta_i = U\left[-\sqrt{3},\sqrt{3}\right]$.

Since the quantified random field Z does not have the desired value for topology optimization, i.e., $Z \notin \left[0,\ 1\right]$, an operation shall be conducted on this field to transform its range to [0,1]. Therefore, the cumulative density function (CDF) is applied to the random field Z, and a new random field $\hat{Z}(\rho,\zeta)$ is obtained [26]:

$$\hat{Z}\left(\rho,\zeta\right) = CDF\left[Z\left(\rho,\zeta\right)\right] \in \left[0,1\right] \tag{14}$$

2.2.2 Uncertainty propagation

In this work, the Sparse Grid Collocation (SGC) method is used for the propagation of uncertainty. Suppose that $Q_l^{(1)}f$ is a family of quadrature rules, and $\Delta_l^{(1)}f$ is also a quadrature rule [31]:

$$\Delta_l^{(1)}f \equiv \left(Q_l^{(1)} - Q_{l-1}^{(1)}\right)f,\ Q_0^{(1)}f \equiv 0\,. \tag{15}$$

For nested formulae, $\Delta_l^{(1)} f$ contains the set of nodes $Q_l^{(1)} f$ with weights equal to the difference of weights between levels l and $(l-0)$. By introducing the multi-index $\boldsymbol{l}=(l_1,...,l_N)\in N^N$, the sparse cubature can be constructed as:

$$|\boldsymbol{l}| \equiv \sum_{i=1}^{N} l_i. \tag{16}$$

At level l, this multi-index is applied, and the sparse cubature formula is represented by:

$$Q_l^{(N)} f \equiv \sum_{|\mathbf{l}|\le l+N-1} \left(\Delta_{l_1}^{(1)} \otimes \cdots \otimes \Delta_{l_N}^{(1)}\right) f, \tag{17}$$

where the multi-index expression of the support nodes is $|\boldsymbol{l}| = l_1 + \ldots + l_d$, and N is the dimension of objective function f. Using a recursive manner, the interpolant can be expressed as:

$$Q_l^{(d)} f = \sum_{l+1\le|\boldsymbol{l}|\le l+d} (-1)^{l+d-|\boldsymbol{k}|} \begin{pmatrix} d-1 \\ l+d-|\boldsymbol{k}| \end{pmatrix} \left(Q_{k_1}^{(1)} \otimes \cdots \otimes Q_{k_d}^{(1)}\right) f. \tag{18}$$

Using the Smolyak algorithm [32], the weight w_i of the i^{th} collocation point ζ_i is defined as:

$$w_i = (-1)^{l+d-|\boldsymbol{k}|} \begin{pmatrix} d-1 \\ l+d-|\boldsymbol{k}| \end{pmatrix} \left(w_{k_1}^{i_1} \otimes \cdots \otimes w_{k_d}^{i_d}\right). \tag{19}$$

Then, the mean and standard deviation of the objective function f can be computed using the SGC method:

$$\begin{aligned} &\mathbb{E}[f] = \sum_k w_k f(Z_k), \\ &\mathrm{Var}[f] = \mathbb{E}\left[f^2\right] - (\mathbb{E}[f])^2. \end{aligned} \tag{20}$$

Note that the weight w_i and collocation point ζ_k is calculated by the sparse grid of the Clenshaw-Curtis type with non-equidistant nodes in this work.

2.2.3 Uncertainty in material property (UNM)

The UNM such as the Young's modulus is usually represented by a random field as follows:

$$E = h\left[\hat{Z}(\rho,\zeta)\right], \tag{21}$$

where $h[]$ is a derivative function. To model the material properties of systems, there are relatively simple and physically acceptable marginal distributions such as uniform distribution, log-normal and beta. In this work, a uniform distribution is adopted to model the Young's modulus as Eq. (22) for uncertainty:

$$\begin{aligned} &E = \rho^p E_m, \\ &E_m = \beta_1 \hat{Z}(\rho,\zeta) + \beta_2, \end{aligned} \tag{22}$$

where E_m is the uniform distribution, and two control parameters β_1 and β_2 are used to confirm the presence of the function $\hat{Z}(\rho,\zeta)$ in the range of zero and one.

2.2.4 Uncertainty in Load (UNL)

Two categories of UNL are considered in this work: the first one is on the loading angle, and the second one is on load amplitude. These uncertainties are determined by two independent random variables. The random field of the loading angle is represented by a uniform distribution, while the uncertainty in the load amplitude is supposed to have a Gaussian distribution with a mean of 1 and a standard deviation (STD) of 0.3. Therefore, these two uncertainties are formulated as:

$$\begin{aligned} &f(\rho,\zeta) = FA(\rho,\zeta), \\ &F = N(1,0.3),\ A(\rho,\zeta) = \sum_{i=1}^{n_{\mathrm{mod}\,e}} \sqrt{\lambda_i}\gamma_i(\rho)\varphi_i(\zeta), \end{aligned} \tag{23}$$

where F and A are the amplitude and angle of the applied load, respectively.

2.2.5 Uncertainty in Geometry (UNG)

Geometric uncertainty in design topology can be modeled by introducing randomness to the threshold η, meaning that the image threshold is modeled as a random variable with a probabilistic distribution. This approach models uncertainty in structures that are fabricated via etching. The etching process causes errors in the form of over- or under-etching which produces structures that are either thinner or thicker than intended. On a more realistic assumption, the etching can cause a non-uniform variation of errors in the design domain. In the present paper, this variation is represented by replacing the random variable η with the random field such that:

$$\eta(x,\zeta) = \alpha_1 \hat{Z}(x,\zeta) + \alpha_2, \tag{24}$$

where $\hat{Z}(x,\zeta) \in [0,1]$ is a random field, α_1 and α_2 controls the mean and range of the process η such that $\eta(x,\zeta) \in [0,1]$.

2.2.6 Optimization algorithm

Finally, after the representation of different uncertainties is completed, the SGC is applied to propagate the uncertainties. The complete algorithm for robust topology optimization is described as follows:

1. Problem discretization and initialization
2. Generation of the KLE by Eq. (13);
3. Application of the adaptive sparse grid method for generating M integration points and the corresponding weights;
4. Optimization process.

Do until convergence:

- For $k = 1, \ldots, M$, compute $\boldsymbol{K}_k \boldsymbol{u}_k = \boldsymbol{f}_k$ and $\frac{\partial C_k}{\partial \rho}$;
- Estimate $\mathbb{E}[C]$ and Var$[C]$ from Eq. (20);
- Evaluate the mean and variance of sensitivities with respect to the design variable;
- Compute the sensitivity of the stochastic compliance from Eq. (11);
- Update $\boldsymbol{\rho}$.

This process is shown in Fig. 1 as a flowchart.

3 Numerical examples

MATLAB software has been used in this work for implementing two numerical examples. In Fig. 2, the first 100 eigenvalues of the correlation matrix R have been illustrated, where their fast modal decay is obvious.

As stated in Section 2.2.1, the expansion should be reduced to the first n_{mode} modes for dimension reduction. For this purpose, the ratio $\left(\sum_{i=1}^{n_{mode}} \lambda_i\right) / \left(\sum_{i=1}^{n} \lambda_i\right)$ is used to determine the first n_{mode} modes for representing the random field. According to Fig. 2, $n_{mode} = 4$ is the best choice, i.e., this truncation yields a 96% representation of Z which is deemed sufficient.

3.1 Example 1: Two-Dimensional-MBB beam

A 2D-MBB beam, one of the most popular examples for RTO, is used as the first example for the comparative study on the HU. The design domain, boundary and loading conditions of this example are depicted in Fig. 3. The geometric parameters of the MBB beam are considered as $L = 90$ mm and $H = 30$ mm, and $T = 1$ mm. The material is assumed to have a Young's modulus of 1 MPa for the solid phase and a Poisson ratio of 0.3.

To help validate the RTO results in Section 3.3, the Deterministic Topology Optimization (DTO) results are first presented in Fig. 4 to show the overall treatment of this MBB beam under the above loading, material and geometric conditions. To study the effect of various uncertainties on the final topology, it is supposed in this example that the loading angle has a uniform distribution in the distance of

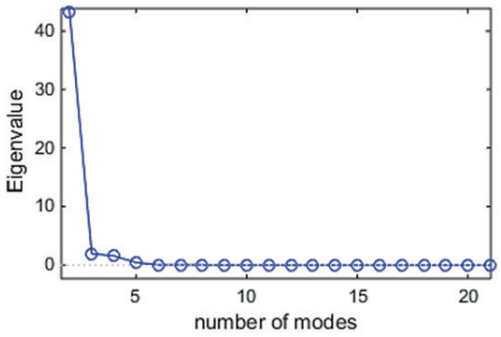

Fig. 2 Correlation eigenvalues of random field Z

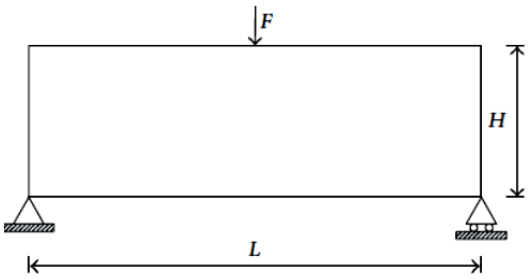

Fig. 3 Design domain, boundary and loading conditions of a 2D MBB beam

Fig. 4 DTO results of a 2D MBB beam (Compliance = 34.63)

[π/4, 3π/4], and the load magnitude follows the Gaussian distribution with an average of 1 and an STD of 0.3. To consider the material uncertainty, it is assumed that the Young's modulus is modeled via a 2D marginally uniform random field. As explained in Section 2.2.5, the geometric uncertainty is modeled by representing the threshold η as a random field with spatially varying manufacturing tolerances.

3.2 Example 2: 2D Cantilever beam

As the second numerical benchmark, a 2D cantilever beam is selected to further investigate the effect of HU on RTO. The design domain, boundary and loading conditions are delineated in Fig. 5. The geometric parameters of the cantilever beam are set as $L = 80$ mm, $H = 30$ mm, and $T = 1$ mm. The material properties are the same as those in Example 1. Two concentrated unit loads are applied on the middle point of the beam end.

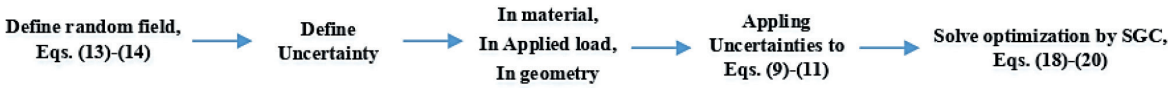

Fig. 1 General problem-solving process

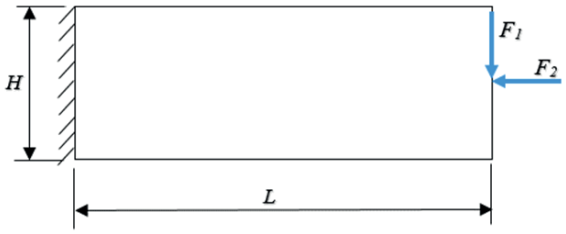

Fig. 5 Design domain, boundary and loading conditions of a 2D cantilever beam

Fig. 6 DTO results of a 2D cantilever beam (Compliance = 1.52)

The DTO results of this cantilever beam are given in Fig. 6 to illustrate its overall handling under the deterministic loading, material and geometric conditions. For RTO analysis, the material and geometric uncertainties are the same as those in Example 1. It is supposed that the load magnitude of F_2 follows the same distribution as that of load magnitude of F in Example 1, while F_1 and the loading angle of F_2 are deterministic.

3.3 RTO results and discussion

In this section, the RTO results of the above two examples with different types of HU and the individual component uncertainties are presented and discussed. For simplicity, the abbreviations of RTO models under different uncertainties are listed in Table 1.

Comparisons of the RTO designs under the various HU (HUML, HUGL, HUMG & HUMGL) and the individual component uncertainties (UNL, UNM & UNG) for two benchmarks are given in Table 2 and Fig. 7, and Table 3 and Fig. 8, respectively.

3.3.1 RTO model with HU in material property and load (HUML)

It is observed from the above results of both examples that the robust design under HUML has intermediate values of mean, STD and compliance compared with those under UNL and UNM, and is more stable than that under the loading uncertainty due to the smaller STD. In other words, the RTO design under this kind of hybrid uncertainty can be considered as a conservative state with a mediocre and realistic prediction.

The higher amount of standard deviation for the case of UNL is a logical expression. This can be explained by the fact that the load, which can be assumed to be a pertur-

Table 1 Abbreviations of RTO models under different uncertainties

RTO model under uncertainty	Abbreviation
Uncertainty in load	UNL
Uncertainty in material property	UNM
Uncertainty in geometry	UNG
Hybrid uncertainties in material property and load	HUML
Hybrid uncertainties in geometry and load	HUGL
Hybrid uncertainties in material property and geometry	HUMG
Hybrid uncertainties in material, geometry, and load	HUMGL

Table 2 Comparison of RTO designs with different uncertainty models for Example 1

RTO model	Mean	STD	Compliance
UNL	19.53	5.59	25.12
UNM	24.81	2.02	26.82
UNG	26.81	2.12	28.93
HUML	21.12	5.02	26.14
HUGL	22.22	4.48	26.70
HUMG	26.37	2.07	28.44
HUMGL	20.82	4.60	25.42

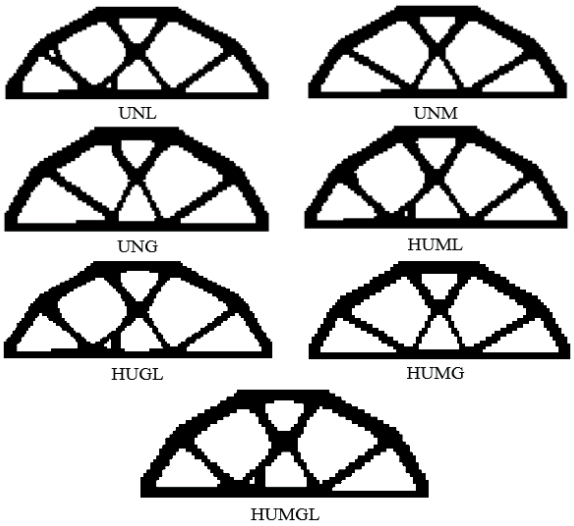

Fig. 7 Optimized topologies obtained with different uncertainty models for Example 1

Table 3 Comparison of RTO designs with different uncertainty models for Example 2

RTO model	Mean	STD	Compliance
UNL	0.86	0.22	1.09
UNM	1.33	0.10	1.42
UNG	1.40	0.10	1.51
HUML	1.13	0.14	1.28
HUGL	1.19	0.11	1.30
HUMG	1.34	0.10	1.44
HUMGL	1.04	0.12	1.17

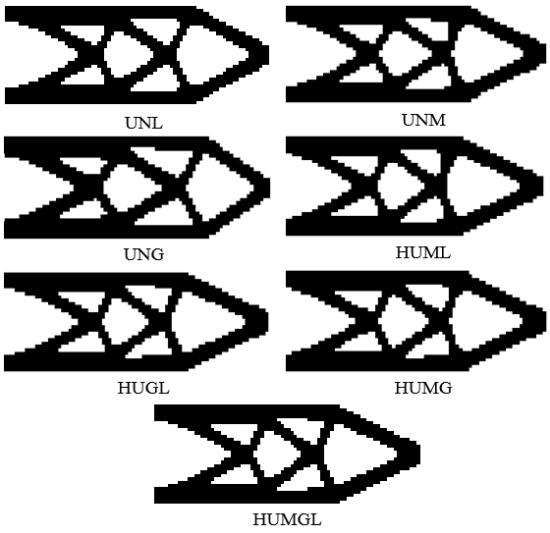

Fig. 8 Optimized topologies obtained with different uncertainty models for Example 2

bation, is an external effect on the structure. For further consideration, it is assumed that we have a system of one degree of freedom. Then, the compliance relation in the form of $C = u^T F$ and $Ku = F$ can be shown as $C = F^2/K$, in which F is the applied load and K is the stiffness. Given this relationship, it is clear that the effect of load on the compliance is much greater than that of other parameters. Therefore, as can be seen from the results of the hybrid state, the STD value is closer to that obtained from the state of UNL.

3.3.2 RTO model with HU in geometry and load (HUGL)

For RTO model under HUGL, it is found that the hybrid model has intermediate values for the RTO designs compared with the two models of component uncertainty. Also, it has a smaller standard deviation compared with the UNL model, indicating that the achieved RTO design is less sensitive to the variations in the hybrid uncertainty model. Note that the above phenomena are similar to those observed in the previous HUML model.

As explained in Section 3.3.1 for the HUML model, the effect of loading uncertainty on the compliance is greater than that of material uncertainty. For the HUGL model, similar conclusion to that of the HUML model can be made, i.e., the effect of loading uncertainty on the compliance is more significant than that of geometric uncertainty. As can be seen in Eq. (2) and Eq. (6), the material properties (Young's modulus and physical density) can be regarded as a function of the parameter η, which not only determines the structural boundary with geometric uncertainty but also indicates the material distribution (e.g., solid or empty phases) of the structure. As a result, the geometric uncertainty may have a similar effect to that of the material uncertainty in the hybrid uncertainty model.

3.3.3 RTO model with HU in material property and geometry (HUMG)

For the third hybrid model of HUMG, it can be seen from the preceding results that the values obtained from this hybrid model are smaller than those from the UNG and larger than those from the UNM. Moreover, it is observed that the results of HUMG tend to those of UNG, which is also attributed to the relationship between the parameter η and the material properties.

3.3.4 RTO model with HU in material property, geometry, and load (HUMGL)

The final model considers the HU in material property, geometry and load. Similarly, it is noticed that the robust design with HUMGL has intermediate values of mean, STD and compliance compared to those with the component uncertainty models. Also, it can be concluded from these results that the loading uncertainty has a greater effect on the compliance than the material and geometric uncertainties in all the involved hybrid models.

4 Conclusions

TO methods have been widely used in structural engineering (for example, aerospace, electronics, biomedical, automotive, and civil engineering) and have improved the quality of final products. However, although currently available studies have led to significant improvements in structural design, in most cases, these investigations are based on deterministic assumptions based on one or more items such as nominal material properties and loading conditions, as well as geometries. The possible sources of uncertainty in TO problems are load conditions and material properties, as well as geometric changes due to observation errors, incomplete information, manufacturing defects, etc., which makes the combination of these matters particularly important.

This paper presents a comparative study on the HU for RTO of continuum structures, in which a truncated KLE is employed for uncertainty representation and a SGC method for uncertainty propagation of the objective function and constraints. The major findings of this study can be summarized as follows:

(1) In the presence of HU, the RTO results tend towards those with UNL only, which is due to the weight effect of load on the compliance as compared with that of material property and geometry ($C = F^T \boldsymbol{u}$);

(2) The combination of loading uncertainty with material or geometric uncertainty leads to the RTO design with a larger standard deviation compared to the cases with single source of uncertainties (either material uncertainty or geometric uncertainty), which may have a negative effect on the stability of the structure;

(3) The hybrid uncertainty model is a relatively conservative state, in which the weakness of a scenario with single uncertainty can be avoided. Since the loading uncertainty causes a larger standard deviation than the uncertainties of other parameters, the final topology may be more sensitive to variations in design variables.

As a result, by combining the loading uncertainty with other sources of uncertainties, the main goal of robust design to alleviate the standard deviation can be achieved.

Acknowledgments

This work was supported by the National Natural Science Foundation of China (Grant No. 11872190) and Research Foundation for Jinshan Distinguished Professorship at Jiangsu University (Grant No. 4111480003).

References

[1] Lógó, J., Ismail, H. "Milestones in the 150-Year History of Topology Optimization: A Review", Computer Assisted Methods in Engineering and Science, 27(2–3), pp. 97–132, 2020. https://doi.org/10.24423/cames.296

[2] Csébfalvi, A. "Structural optimization under uncertainty in loading directions: Benchmark results", Advances in Engineering Software, 120, pp. 68–78, 2018. https://doi.org/10.1016/j.advengsoft.2016.02.006

[3] Pintér, E., Lengyel, A., Lógó, J. "Structural Topology Optimization with Stress Constraint Considering Loading Uncertainties", Periodica Polytechnica Civil Engineering, 59(4), pp. 559–565, 2015. https://doi.org/10.3311/PPci.8848

[4] Dániel, H., Habashneh, M., Rad, M. M. "Reliability-based numerical analysis of glulam beams reinforced by CFRP plate", Scientific Reports, 12, 13587, 2022. https://doi.org/10.1038/s41598-022-17751-6

[5] Rad, M. M. "A Review of Elasto-Plastic Shakedown Analysis with Limited Plastic Deformations and Displacements", Periodica Polytechnica Civil Engineering, 62(3), pp. 812–817, 2018. https://doi.org/10.3311/PPci.11696

[6] Kharmanda, G., Olhoff, N., Mohamed, A., Lemaire, M. "Reliability-based Topology Optimization", Structural and Multidisciplinary Optimization, 26, pp. 295–307, 2004. https://doi.org/10.1007/s00158-003-0322-7

[7] Csébfalvi, A., Lógó, J. "A critical analysis of expected-compliance model in volume-constrained robust topology optimization with normally distributed loading directions, using a minimax-compliance approach alternatively", Advances in Engineering Software, 120, pp. 107–115, 2018. https://doi.org/10.1016/j.advengsoft.2018.02.003

[8] Rad, M. M. "Reliability Based Analysis and Optimum Design of Laterally Loaded Piles", Periodica Polytechnica Civil Engineering, 61(3), pp. 491–497, 2017. https://doi.org/10.3311/PPci.8756

[9] Rad, M. M., Habashneh, M., Lógó, J. "Elasto-Plastic limit analysis of reliability based geometrically nonlinear bi-directional evolutionary topology optimization", Structures, 34, pp. 1720–1733, 2021. https://doi.org/10.1016/j.istruc.2021.08.105

[10] Maute, K. "Topology optimization under uncertainty", In: Topology Optimization in Structural and Continuum Mechanics, Springer, 2014, 457–471. ISBN 978-3-7091-1642-5 https://doi.org/10.1007/978-3-7091-1643-2_20

[10] Elishakoff, I., Haftka, R. T, Fang. J. "Structural design under bounded uncertainty - Optimization with anti-optimization", Computers & Structures, 53(6), pp. 1401–1405, 1994. https://doi.org/10.1016/0045-7949(94)90405-7

[12] Dunning, P. D., Kim, H. A., Mullineux, G. "Introducing loading uncertainty in topology optimization", AIAA Journal, 49(4), pp. 760–768, 2011. https://doi.org/10.2514/1.J050670

[13] Cai, J., Wang, C., Fu, Z. "Robust concurrent topology optimization of multiscale structure using single or multiple uncertain load cases", International Journal for Numerical Methods in Engineering, 121(7), pp. 1456–1483, 2020. https://doi.org/10.1002/nme.6275

[14] Latifi Rostami, S. A., Kolahdooz, A., Zhang, J. "Robust topology optimization under material and loading uncertainties using an evolutionary structural extended finite element method", Engineering Analysis with Boundary Elements, 133, pp. 61–70, 2021. https://doi.org/10.1016/j.enganabound.2021.08.023

[15] Guest, J. K., Igusa, T. "Structural Optimization Under Uncertain Loads and Nodal Locations", Computer Methods in Applied Mechanics and Engineering, 198(1), pp. 116–124, 2008. https://doi.org/10.1016/j.cma.2008.04.009

[16] Lógó, J. "New type of optimality criteria method in case of probabilistic loading conditions", Mechanics Based Design of Structures and Machines, 35(2), pp. 147–162, 2007. https://doi.org/10.1080/15397730701243066

[17] Lógó, J. "SIMP type topology optimization procedure considering uncertain load position", Periodica Polytechnica Civil Engineering, 56(2), pp. 213–219, 2012. https://doi.org/10.3311/pp.ci.2012-2.07

[18] Lógó, J., Ghaemi, M., Rad, M. M. "Optimal Topologies in Case of Probabilistic Loading: The Influence of Load Correlation", Mechanics Based Design of Structures and Machines, 37(3), pp. 327–348, 2009. https://doi.org/10.1080/15397730902936328

[19] Tootkaboni, M., Asadpoure, A., Guest, J. K. "Topology optimization of continuum structures under uncertainty - A polynomial chaos approach", Computer Methods in Applied Mechanics and Engineering, 201, pp. 263–275, 2012. https://doi.org/10.1016/j.cma.2011.09.009

[20] da Silva, G. A., Cardoso, E. L. "Topology optimization of continuum structures subjected to uncertainties in material properties", International Journal for Numerical Methods in Engineering, 106(3), pp. 192–212, 2016. https://doi.org/10.1002/nme.5126

[21] Agrawal, G., Gupta, A., Chowdhury, R., Chakrabarti, A. "Robust topology optimization of negative Poisson's ratio metamaterials under material uncertainty", Finite Elements in Analysis and Design, 198, 103649, 2022. https://doi.org/10.1016/j.finel.2021.103649

[22] Zhang, W., Kang, Z. "Robust shape and topology optimization considering geometric uncertainties with stochastic level set perturbation", International Journal for Numerical Methods in Engineering, 110(1), pp. 31–56, 2017. https://doi.org/10.1002/nme.5344

[23] Latifi Rostami, S. A., Ghoddosian, A. "Robust Topology Optimization under Load and Geometry Uncertainties by Using New Sparse Grid Collocation Method", Periodica Polytechnica Civil Engineering, 63(3), pp. 898–907, 2019. https://doi.org/10.3311/PPci.13077

[24] Latifi Rostami, S. A., Ghoddosian, A. "Topology Optimization Under Uncertainty by Using the New Collocation Method", Periodica Polytechnica Civil Engineering, 63(1), pp. 278–287, 2019. https://doi.org/10.3311/PPci.13068

[25] Latifi Rostami, S. A., Ghoddosian, A., Kolahdooz, A., Zhang, J. "Topology optimization of continuum structures under geometric uncertainty using a new extended finite element method", Engineering Optimization, 54(10), pp. 1692–1708, 2022. https://doi.org/10.1080/0305215X.2021.1957860

[26] Latifi Rostami, S. A., Ghoddosian, A. "Topology optimization of continuum structures under hybrid uncertainties", Structural and Multidisciplinary Optimization, 57(6), pp. 2399–2409, 2018. https://doi.org/10.1007/s00158-017-1868-0

[27] He, Z. C., Wu, Y., Li, E. "Topology optimization of structure for dynamic properties considering hybrid uncertain parameters", Structural and Multidisciplinary Optimization, 57(2), pp. 625–638, 2018. https://doi.org/10.1007/s00158-017-1769-2

[28] Meng, Z., Wu, Y., Wang, X., Ren, S., Yu, B. "Robust topology optimization methodology for continuum structures under probabilistic and fuzzy uncertainties", International Journal for Numerical Methods in Engineering, 122(8), pp. 2095–2111, 2021. https://doi.org/10.1002/nme.6616

[29] Bai, S., Kang, Z. "Robust topology optimization for structures under bounded random loads and material uncertainties", Computers & Structures, 252, 106569, 2021. https://doi.org/10.1016/j.compstruc.2021.106569

[30] Cheng, J., Lu, W., Liu, Z., Wu, D., Gao, W., Tan, J. "Robust optimization of engineering structures involving hybrid probabilistic and interval uncertainties", Structural and Multidisciplinary Optimization, 63(3), pp. 1327–1349, 2021. https://doi.org/10.1007/s00158-020-02762-6

[31] Lazarov, B. S., Schevenels, M., Sigmund, O. "Topology optimization considering material and geometric uncertainties using stochastic collocation methods", Structural and Multidisciplinary Optimization, 46(4), pp. 597–612, 2012. https://doi.org/10.1007/s00158-012-0791-7

[32] Keshavarzzadeh, V., Fernandez, F., Tortorelli, D. A. "Topology optimization under uncertainty via non-intrusive polynomial chaos expansion", Computer Methods in Applied Mechanics and Engineering, 318, pp. 120–147, 2017. https://doi.org/10.1016/j.cma.2017.01.019